Active microrheology of networks composed of semiflexible polymers: Theory and comparison with simulations

N. Ter-Oganessian,[1] D. A. Pink,[2] and A. Boulbitch[1]
[1]*Department for Biophysics E22, Technische Universität München, James-Franck-St., D-85747 Garching bei München, Germany*
[2]*Physics Department, St. Francis Xavier University, Antigonish, Nova Scotia, Canada B2G 2W5*
(Received 24 March 2005; revised manuscript received 5 July 2005; published 24 October 2005)

Based on the results of our computer simulation [Ter-Oganessian *et al.*, Phys. Rev. E **72**, 041510 (2005)], we have developed a theoretical description of the motion of a bead, embedded in a network of semiflexible polymers (filaments) and responding to an applied force. The theory reveals the existence of an osmotic restoring force, generated by the piling up of filaments in front of the moving bead and first deduced through computer simulations. The theory predicts that the bead displacement scales like $x \sim t^{\alpha}$ with time, where $\alpha = 1/2$ in an intermediate-time regime and $\alpha = 1$ in a long-time regime. It also predicts that the compliance varies with a concentration like $c^{4/3}$ in agreement with experiment.

DOI: 10.1103/PhysRevE.72.041511 PACS number(s): 83.10.Kn, 87.16.Ka, 83.60.Bc, 82.35.Pq

I. INTRODUCTION

Actin networks play a key role in the mechanical stability of cells and for numerous mechanochemical processes [2], such as cell locomotion on surfaces [3] and the growth of cellular protrusions [4]. The viscoelastic properties of actin networks have been extensively studied by torsional rheometry [5–8], passive one-bead [9,10] and two-bead [11] microrheology and force-based (oscillatory) microrheometry [12,13].

Recently, new results using pulsed force magnetic bead microrheometry were reported [14,15] in which three regimes of bead movement were observed, each being described by the power law

$$x(t) \sim t^{\alpha_i}, \tag{1}$$

where x is the bead displacement and t is the time and i numerates the regimes $i=1,2,3$: the short-time regime with the exponent $\alpha_1 \approx 0.75$ observed for $0 \leqslant t \leqslant \tau_1$; the intermediate-time regime characterized by $\alpha_2 \approx 0.5$, for $\tau_1 \leqslant t \leqslant \tau_2$, and the long-time viscous-like regime, for $t > \tau_2$, with the exponent $\alpha_3 \approx 1$. The crossover time τ_1 varied between 0.03 and 0.3 s, while τ_2 varied between 10 and 30 s depending on the force applied to the bead. In the intermediate-time and long-time regimes, the dependence of bead displacement on the concentration of actin filaments c behaved like $x \sim c^{-\gamma_i}$ with $\gamma_2 \approx 1.1 \pm 0.3$ in the intermediate-time regime and $\gamma_3 \approx 1.3 \pm 0.3$ in the long-time regime [14].

Actin networks and constrained actin filaments were studied theoretically in a series of papers [5,6,16–31] and theoretical analyses of microrheology have recently been reported in [32–34]. Up to now, no theoretical explanation of the $x(t) \sim t^{1/2}$ power law of the bead motion in active microrheology of semiflexible entangled networks has been proposed.

In the preceding paper [1], we reported the results of computer simulation of magnetic bead microrheometry to study a network of semiflexible polymers modeling entangled actin filaments in an aqueous solution. In Fig. 1, we show some typical results of computer simulations using the parameters of the paper [1]. Figure 1(a) shows a typical plot of $\log[x(t)]$ versus $\log(t)$. Two regimes of bead motion can be distinguished on this graph. The initial regime was characterized by the well-known exponent $\alpha_1 \approx 0.75$ [9,11,21,23–25]. The displacement of the bead in this regime observed in the computer simulations [1] was smaller than the network mesh size in accord with the observations [14]. This was followed by the regime with the exponent $\alpha_2 \approx 0.5$ [Fig. 1(a)]. In this regime, the displacement can be represented in the form $x(t) = Kt^{1/2}$, where the coefficient K depends upon the concentration of filaments c, like $K \sim c^{-\gamma_2}$ with $\gamma_2 \approx 1.4$ [Fig. 1(b)]. It was further shown [1] that the bead displacement in this regime scales like

$$x(t) \sim D_{\parallel}^{1/2} f t^{\alpha_2} c^{-\gamma_2}, \tag{2}$$

where f is the external force applied to the bead and $D_{\parallel}$ is the longitudinal diffusion coefficient defined as the diffusion coefficient of a polymer constrained to move along its tube [28]. A total displacement of several mesh sizes was achieved by the end of the simulation. The two regimes observed in the simulations correspond to the short-time and intermediate-time regimes observed using pulsed force magnetic bead microrheometry [14,15] and are characterized by the same exponents.

Figure 1(c) shows the number of monomers N_m neighboring the leading and the rear hemispheres of the bead. These numbers were equal in the rest state ($t=0$). During the bead motion the number of the monomers neighboring the leading hemisphere increased [Fig. 1(c)(i)] while the number of those neighboring the rear hemisphere decreased [Fig. 1(c)(ii)]. This implied that, during bead motion in the intermediate-time regime, the polymers piled up in front of the bead, while the region behind the bead was almost free of polymers. Further, the simulations demonstrated that the resistance of the network to bead motion was due mainly to the steric repulsion of these piled up polymers [as shown in Fig. 1(d)]. Finally, the simulations [1] showed that the polymers in front of the bead take part, on average, in a diffusive motion in the direction of the bead motion. The diffusion

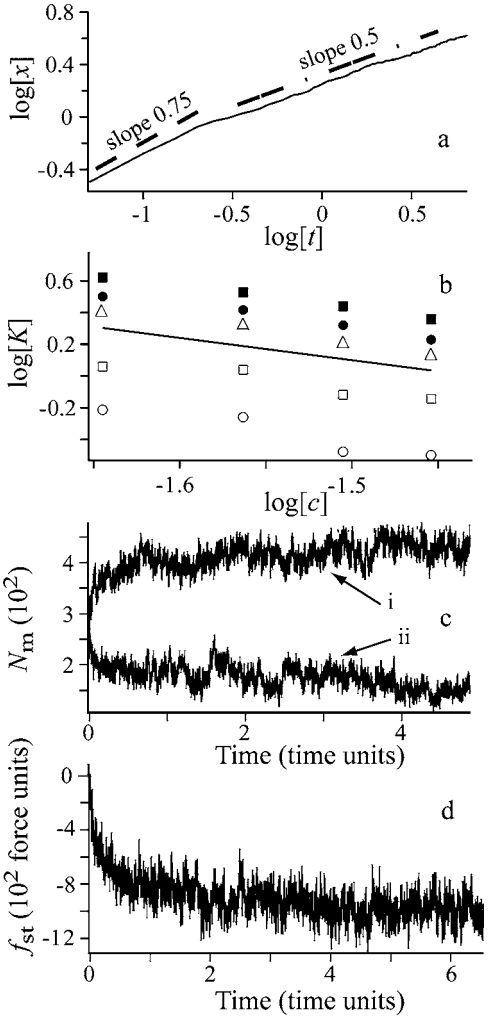

FIG. 1. Results of computer simulations of magnetic bead microrheometry of an actin network [1]. (a) Typical dependence of the bead displacement $x(t)$ versus time t in a double-logarithmic plot revealing two regimes of bead motion: the initial regime characterized by the slope $\alpha_1 \approx 0.75$ followed by that with the slope $\alpha_2 \approx 0.5$. The dashed and dashed-dotted lines show the slopes 3/4 and 1/2, respectively. (b) The double-logarithmic plot of the dependence of the coefficient K on the concentration of filaments c at various forces. The solid line shows the slope $\gamma_2 = -1.4$. (c) The numbers of monomers N_m neighboring the leading (i) and the rear (ii) hemispheres of the bead plotted versus time. (d) The steric repulsion force f_{st} exerted by the filaments on the bead plotted versus time. In this simulation, an external force of 1000 force units was applied to the bead. The force f_{st} gradually increased in magnitude from $f_{st}=0$ at $t=0$ to $f_{st} \approx -1000$ force units, thus balancing the external force at $t \gtrsim 2$ time units which corresponds to the intermediate regime.

coefficient of this motion is close to the longitudinal diffusion coefficient describing the free diffusion of polymers in the bulk [1].

Based on these findings, this paper formulates an analytical approach deriving the intermediate-time and the long-time regimes and describing both the experimental observations [14,15] and the results of our simulations [1].

In Sec. II, we deduce the force resisting the bead motion on the assumption that a clump of polymers has been formed in front of the moving bead. In Sec. III, we describe the formation of the clump and obtain equations of motion of the bead in the intermediate-time regime. In Sec. IV, we extend our approach to describe the long-time regime of bead motion. In Sec. V, we compare our predictions with measurements and simulations and discuss the relation of our findings to previous experimental and theoretical results. Section VI summarizes our results.

II. OSMOTIC FORCE

Actin networks are well described by a reptation-tube model [26,27]. Within this approach, each filament is considered to be confined to a tube with diameter equal to the mesh size accounting for the steric contribution of the surrounding filaments. This yields the free energy per filament [17,19,20,35]

$$F_f \approx \kappa k_B T L / L_e, \tag{3}$$

where $\kappa \approx 2.46$ is a geometric factor, $L_e \sim L_p^{1/3} \xi^{2/3}$ is the entanglement length [16], and L_p is the persistent length of the filament. The term originating from the translational entropy of the filaments is omitted in (3), since its effect on the resistive force is small.

In a system with N polymers of length L homogeneously distributed in volume V, the mesh size of the network ξ can be estimated according to the relation $V = gNL\xi^2$, where g is a geometric factor. The concentration of the polymers is defined as $c = N/V$ yielding

$$c = 1/gL\xi^2. \tag{4}$$

In the following it is convenient to write all expressions in terms of the concentration c^* of segments of filaments with length L_e according to the definition $c^* = cL/L_e$,

$$c^* = 1/gL_p^{1/3}\xi^{8/3}. \tag{5}$$

These segments play an important role in our discussion and, therefore, for the sake of brevity, we introduce a special term, "entanglement segments," for them. According to (3) each entanglement segment carries the thermal energy $\sim \kappa k_B T$.

The free energy of the network takes the form $F = NF_f$,

$$F \sim k_B T \left[\frac{(LN)^4}{L_p V} \right]^{1/3}. \tag{6}$$

Making use of Eq. (6), one calculates the pressure $p = -(\partial F/\partial V)_T$ and using Eq. (5) one finds,

$$p \sim c^* k_B T. \tag{7}$$

The pressure (7) depends on the mesh size like $p \sim \xi^{-8/3}$. It arises due to the decrease of entropy of a filament subjected to a tube. It can be considered as the osmotic pressure of the entanglement segments.

The beads used in the measurements [14,15] and modeled in the simulations [1] are about 5 to 10 times larger than the mesh sizes of the networks and cannot squeeze through the

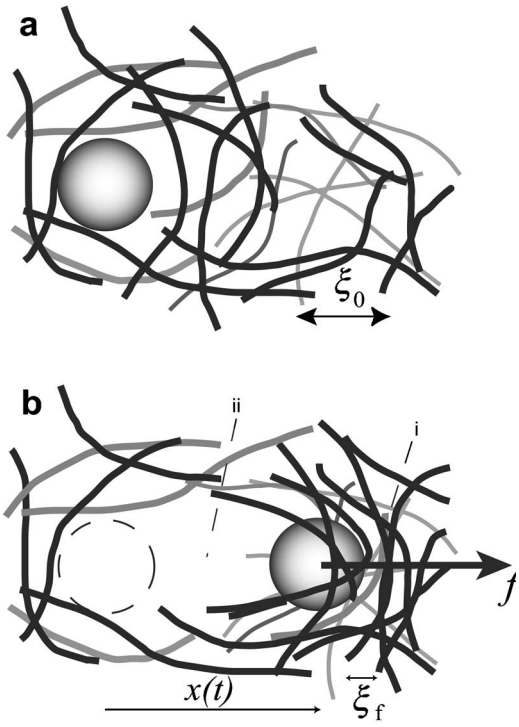

FIG. 2. Schematic view of the bead embedded in a network of semiflexible filaments. (a) Bead at rest in a network. (b) During its motion, the bead piles up the filaments ahead of it (i), while the region behind the bead (ii) contains fewer filaments. The dashed circle shows the initial position of the bead, ξ_f indicates the mesh size in the vicinity of the bead, and ξ_0 is the mesh size far from the bead.

network. For this reason during its motion, the bead compresses the network ahead of it, thus increasing the local concentration of filaments (Fig. 2). The mesh size in front of the bead, $\xi=\xi_f$ [Fig. 2(b)], thus, becomes smaller than the mesh size, $\xi=\xi_0$, far from the bead [Fig. 2(a)].

It has been shown by the simulations that the main contribution to the resistance is due to the steric repulsion between the bead and filaments, which gives rise to the pressure p exerted by the filaments on the bead surface [1]. Further, the simulations show that the filaments are piled up in front of the bead, while behind the bead a region almost free of filaments develops during its motion [1], and hence, it is a good approximation that essentially zero pressure is exerted by filaments on the back hemisphere. Thus, the force $f\sim R^2p$, where R is the bead radius, acts on the front surface of the bead and resists the bead motion. One finds

$$f \sim R^2 c_f^* k_B T, \tag{8}$$

where $c_f^*=1/gL_p^{1/3}\xi_f^{8/3}$ is the concentration of the entanglement segments in the neighborhood of the front of the bead (i.e., in the region where the mesh size ξ is equal to ξ_f). The force (8) represents the steric repulsion of the bead by the polymers piled up in front of it. It is related to the osmotic pressure of the entanglement segments, and we refer to it as the "osmotic force."

III. EQUATION OF MOTION OF THE BEAD: THE INTERMEDIATE-TIME REGIME

In the beginning of the motion, when $t<\tau_1$, the bead response is due to a dynamic bending of a few filaments and obeys the law [21] $x(t)\sim t^{3/4}$ (see Appendix).

At $t>\tau_1$, the short-time regime is followed by the intermediate-time regime in which the bead motion depends upon the response of a large number of those filaments ahead of the bead and crossing the bead's path. The main contribution to the resistance force is described by (8). The concentration of entanglement segments c_f^* entering Eq. (8) is to be calculated directly in front of the bead and should be related to the concentration of segments c_0^* (or to the filament concentration c_0) far from the bead. The latter values are set by the preparation of the network, and we assume them to be known. Basing on the simulations [1], we also assume that the entanglement segments move by diffusion with the diffusion coefficient D.

Consider a bead moving over a distance $x(t)$ during the time t. The bead compresses n_+ entanglement segments ahead of it given by $n_+\sim c_0^*\pi R^2 x(t)$, where $c_0^*=g^{-1}L_p^{-1/3}\xi_0^{-8/3}$ is the concentration of the entanglement segments far from the bead, where the mesh size is ξ_0. These entanglement segments, however, redistribute themselves by diffusing over a typical distance $\sim(Dt)^{1/2}$. If $\tau_1<t<\tau_2$, where

$$\tau_2 \sim R^2/D, \tag{9}$$

there is not enough time for the entanglement segments to diffuse over the distance $\sim R$ away from the bead's path. Therefore, one needs to consider only the diffusion of entanglement segments in the Ox direction. This motion results in a clump of filaments of thickness $\sim(Dt)^{1/2}$ formed in front of the bead so that the entanglement segments redistribute themselves over the volume

$$\delta V \sim \pi R^2 (Dt)^{1/2}. \tag{10}$$

Accordingly, the concentration, $c_f^*\sim n_+/\delta V$, in the clump in front of the bead is

$$c_f^* \sim \frac{x(t)}{(Dt)^{1/2}} c_0^*. \tag{11}$$

Substitution of (11) into the resistive force (8) and assumption that the external force f applied to the bead is balanced solely by the osmotic force f_{osm} (8) yields the equation describing the bead motion during the time interval $\tau_1<t<\tau_2$,

$$x(t) = \chi_2 \frac{L_p^{1/3}\xi_0^{8/3}D^{1/2}}{R^2 k_B T} f t^{1/2}, \tag{12}$$

where χ_2 is a numeric factor of the intermediate regime ($i=2$). Its origin and value are discussed in Sec. V.

IV. THE LONG-TIME REGIME OF BEAD MOTION

If $t>\tau_2$, the polymers have enough time to diffuse over the distance $\sim R$. This enables some entanglement segments

to escape from the path of the bead. In this case, the motion of the bead becomes a steady-state motion as soon as the number of the entanglement segments n_+ being captured by the clump in front of the bead becomes equal to the number n_- diffusing sideways away from the bead's path. As soon as this regime is achieved, the bead moves with a constant velocity v. The number of entanglement segments compressed by the bead within the time t can be estimated as

$$n_+ \sim c_0^* R^2 v t. \tag{13}$$

The flux of entanglement segments is $\mathbf{j}=-D\nabla c^*$. In this regime, the only relevant length scale is the bead size $\sim R$. Accordingly the size of the clump l, both along and perpendicular the Ox direction, can be estimated as $l \sim R$. The gradient of the concentration of the entanglement segments ∇c^* can be estimated as $(c_0^*-c_f^*)/R$. Assuming $c_0^* \ll c_f^*$, one finds an estimate of the flux of segments diffusing away from the clump to be of the form $j \sim D c_f^*/R$. The number of entanglement segments diffusing sideways away from the bead's path is

$$n_- \sim R l j t. \tag{14}$$

Applying the condition of steady-state motion, $n_+=n_-$, one finds the concentration of the entanglement segments in the clump c_f^* to be

$$c_f^* \sim R c_0^* v/D. \tag{15}$$

Substitution of the concentration (15) into the expression for the resistive force (8), one finds

$$f_{osm} \sim \frac{c_0^* k_B T R^3}{D} v. \tag{16}$$

The motion of filaments in the long-time regime is associated with some energy dissipation. The latter can be described by the dissipative function

$$Q = \frac{\zeta}{2} \int c v^2 \, dV, \tag{17}$$

where ζ is the inverse mobility of a filament related to its diffusion coefficient as $\zeta=k_BT/D$, c is the concentration of filaments (which should not be confused with the concentration c^* of the entanglement segments), and v is the velocity of a filament. The integration is over the entire volume of the network.

The motion in the long-time regime takes place with a constant velocity v as the bead pushes a clump of filaments with dimensions $\sim R \times R \times R$ ahead of it. The concentration c of filaments inside the clump is larger than their concentration c_0 far from the clump. It is convenient to consider the problem in the coordinate system moving with the bead. In this system, the bead and the clump are motionless, while the filaments with the concentration c_0 fall on the clump with the velocity v and the same amount of polymers leaves the clump providing dynamic equilibrium. Thus, this process can be considered as if the filaments with concentration c_0 move through the clump with the velocity v. The energy dissipation takes place mainly inside the clump. Therefore, the integral (17) can be estimated as $\int c v^2 \, dV \sim c_0 v^2 R^3$. This yields the estimate for the dissipative function $Q \sim v^2 k_B T c_0 R^3/D$. The drag force acting on the bead due to this dissipation takes the form [36] $f_{dis}=-\partial Q/\partial v$. One finds

$$|f_{dis}| \sim \frac{c_0}{c_0^*} \frac{c_0^* k_B T R^3}{D}, \tag{18}$$

where, for the sake of comparison, the force is expressed in terms of the concentration of the entanglement segments c_0^*. Comparing (18) and (16), one finds that $f_{dis}/f_{osm} \sim c_0/c_0^*$. The ratio $c_0/c_0^*=L_e/L=L_p^{1/3}\xi_0^{2/3}/L$ ranges from 0.06 at $\xi_0=0.3$ μm to 0.12 at $\xi_0=1$ μm so that the effects of energy dissipation can be neglected.

For this reason, one can assume that the external force f acting on the bead is balanced only by the osmotic force (16). This yields the equation for steady-state motion,

$$x(t) = x_0 + \chi_3 \frac{L_p^{1/3} \xi_0^{8/3} D}{R^3 k_B T} f t, \tag{19}$$

where x_0 is a constant and χ_3 is the numerical factor which contains all numerical coefficients.

V. DISCUSSION

A. Diffusion coefficient of entanglement segments

Results of our simulation study [1] indicate that the dilatation mode of motion of the clump in front of the bead is diffusive and its diffusion coefficient D is close to that of the longitudinal diffusion of filaments $D_\parallel$. On the other hand, the transverse motion of the filaments in front of the bead leading to a compression or dilatation of this region is more plausible. The transverse motion differs considerably from the longitudinal diffusion [1,37].

This seeming contradiction can be explained as follows. A segment of a filament which crosses the bead's path has the length of about 5 μm. This is smaller than the filament contour length ($\approx$20 μm). For this reason, a clump of polymers in front of the bead is connected by filament tails with the rest of the network, these tails being longer than the size of the clump (Fig. 3). When the bead compresses the clump during its motion, the segments of those filaments in the clump undergo mainly a transverse motion. However, in order to enable such a motion, a longitudinal displacement of the tails (connecting the clump with the network) along their reptation tubes is required. This is shown schematically in Figs. 3(b) and 3(f). Since the lengths of the tails are larger than the clump size, the clump compression by the bead is dominated by the longitudinal diffusion of filaments. For this reason, the diffusion coefficient describing the dynamics of compression of filaments in front of the bead is close to the longitudinal diffusion coefficient of filaments $D \approx D_\parallel$. This conclusion agrees with results of the simulation [1].

B. Distribution of the filaments in the neighborhood of the bead

During the short-time regime, $t < \tau_1$, the clump of polymers ahead of the bead exhibits an increase in density until $t=\tau_1$ after which the density remains constant. This can be seen in Fig. 5 of our simulations [1]. During the intermediate

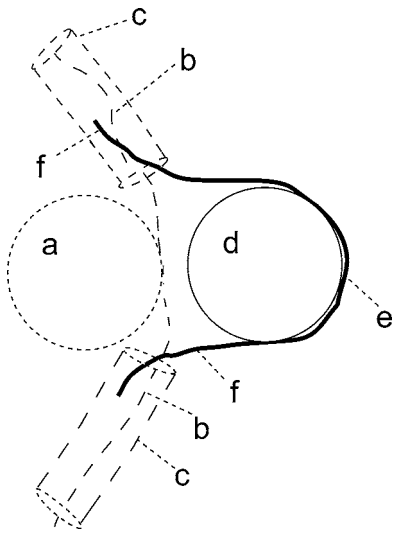

FIG. 3. Motion of a filament crossing the bead's path. An initial position of the bead is shown by (a). (b) shows the tails of one of the filaments which crosses the bead's path in front of it. Other such filaments are not shown. The network (not shown) gives rise to the reptation tubes (c) in which the tails move. Displacement of the bead to a new position [indicated by (d)] requires the movement of those segments crossing the bead's path (e). This requires that the tails slip out of their tubes, thus adopting a new configuration (f).

regime, $\tau_1 < t < \tau_2$, the volume of the clump ahead of the bead Eq. (10), possessing a now-constant density, increases like $t^{1/2}$ and it is this that results in the slowing down of the bead $[x(t) \sim t^{1/2}]$ until $t = \tau_2$. At longer times, a constant speed is maintained $x(t) \sim t$ and the density remains at the value achieved at τ_1. This picture is supported by the theory: a comparison of Eqs. (11) and (12) shows that the concentration of the entanglement segments c_f^* during the intermediate regime is time independent. In our model, the external force f applied to the bead is balanced solely by the osmotic force. According to the relation (8), the concentration c_f^* is unambiguously determined by the time-independent force f.

The evolution of the clump of the filaments in front of the bead, however, takes place by the growth of the clump in the direction of the bead motion $l \sim (Dt)^{1/2}$. Since the number of the segments n_- diffusing away from the clump is proportional to this dimension (14), the growth of the clump is followed by the increase of the number of the escaping segments and stops as soon as this number becomes equal to the number n_+ of segments captured by the clump. From these arguments, one concludes that the concentration c_f^* during the long-time regime (15) is constant and equal to that during the intermediate regime, which is indeed the case.

It is generally accepted that entropic repulsion of a polymer from a chemically neutral surface [38] gives rise to the formation of a depletion layer in which the polymer concentration close to the surface is lower than that in the bulk and a similar manifestation will be seen in the case of a bead embedded in a network of actin filaments [28]. It has been shown that such a depletion layer modifies the elastic Green's function [34] and should be accounted for in analysis of the experimental data of the two-point microrheology [39,40]. In our previous paper [1], we reported the distribution of the polymers in the neighborhood of the bead obtained by simulation. It exhibited an anisotropic distribution of polymers around the bead with a region behind the bead almost free of polymers and a polymer clump in front of it. The simulations did not exhibit any clear indication of a depletion layer around the bead. However, in the simulation [1], soft spheres were used to model the bead and the monomers. In order to identify a depletion layer, we would have to carry out an examination of our simulation data in more detail.

The intent of the work described here has been to model the various time domains in order to understand the key processes which lead to the behavior observed both experimentally and via computer simulation. Our model of the neighborhood of the bead does not take into account phenomena on the scale of a depletion layer, but concerns itself with identifying larger scale processes which lead to the time-dependence observed.

In the framework of our approach, the concentration should be understood as an average rather than an exact value exhibiting any spatial dependence which would reflect a depletion layer. To elucidate fine details of the distribution of the polymers in the vicinity of the bead, a more detailed analysis is required, which is out of the scope of our work.

C. Coefficients χ_2 and χ_3

To make comparisons with experimental data it would be useful to know the values of the coefficients χ_2 and χ_3. In the preceding paper [1], we determined the coefficient χ_2 using the results of our simulations, $\chi_2 \approx 0.055 \pm 0.0042$. This value should be considered as being close to the low limit, since it was obtained for an initially homogenous network composed of polymers with equal contour lengths. Our simulations [1] were not run for sufficiently long times to reach the long-time regime and, accordingly, we were unable to obtain a value for χ_3. However, using data from the literature, we can obtain an estimate for it.

Lekkerkerker and Drohnt calculated the drag force acting on a tracer sphere forced to move with a constant velocity in an emulsion [41]. This drag force is due to the deformation of the particle distribution around the sphere and is, thus, analogous to the osmotic force in the long-time regime considered here. Within the approximation of hard spheres Lekkerkerker and Drohnt found an expression for the osmotic force f_{osm} in terms of the force f applied to the tracer bead

$$f_{\mathrm{osm}} = -\frac{8\pi}{3} R^3 c f, \tag{20}$$

where R is the radius of the tracer (which in the paper [41] is equal to that of the emulsion particles) and c is the concentration of the particles.

If we derive the expression for f_{osm} by making use of (19), we find that $f_{\mathrm{osm}} = -c_0^* R^3 k_B T v g / \chi_3 D$. Taking into account that $v = bf$ and that the mobility b is related to the diffusion coefficient via $D = k_B T b$ one finds the relation

$$f_{\mathrm{osm}} = -\frac{c_0^* R^3 g}{\chi_3} f, \tag{21}$$

to be analogous to the result (20) of Lekkerkerker and Drohnt. Comparison of (20) and (21) yields $\chi_3 = 3g/8\pi$. If the filaments of the network lie along a primitive cubic lattice, one would find $g = 1/3$, which we will use below in making estimates. With this g value one finds that $\chi_3 \approx 0.040$. This value is similar to that obtained by us for χ_2. However, it should be pointed out that the system studied in the paper [41] differs from that considered here and, thus, the value χ_3 may differ from the obtained estimate.

D. Comparison with experiments

The creep compliance of the bead embedded into the actin network $J(t)$ defined by

$$J(t) = 6\pi R x(t)/f \tag{22}$$

was measured in the experiments reported in [14,15]. It was found that, in each of the three regimes, the compliance could be described by the power law

$$J(t) = A_i t^{\alpha_i} + B_i, \tag{23}$$

where A_i are the amplitudes, B_i with $B_1 = B_2 = 0$ are the offsets, and $i = 1,2,3$ denotes the short-time, intermediate-time, and long-time regimes characterized by the exponents $\alpha_1^{(\mathrm{exp})} \approx 0.75$, $\alpha_2^{(\mathrm{exp})} \approx 0.5$, and $\alpha_3^{(\mathrm{exp})} \approx 1.0$ [14,15].

In Sec. III and in the Appendix, these regimes are described analytically. Our estimates on the short-time regime [Eq. (33) Appendix] reproduces the well-known [21] exponent $\alpha_1^{(\mathrm{th})} = 3/4$. In the long-time regime, we obtained the expected exponent $\alpha_3^{(\mathrm{th})} = 1$ [Eq. (19)] describing the viscous-like motion of the bead. Finally in the intermediate-time regime, we derived the exponent $\alpha_2^{(\mathrm{th})} = 1/2$ [Eq. (12)] in agreement with the observations reported in [14,15] as well as our simulations [1]. The theory presented here predicts the prefactors A_i to take the forms

$$A_1 \approx \frac{RN}{32}\left[\frac{\pi}{k_B T L_{\mathrm{p}} (4\eta)^3}\right]^{1/4}, \tag{24}$$

$$A_2 \approx 6\pi\chi_2 \frac{L_{\mathrm{p}}^{1/3} \xi_0^{8/3} D^{1/2}}{R k_B T}, \tag{25}$$

$$A_3 \approx 6\pi\chi_3 \frac{L_{\mathrm{p}}^{1/3} \xi_0^{8/3} D}{R^2 k_B T}, \tag{26}$$

where η is the water viscosity and N is the number of filaments met by the bead (see Appendix).

Since, according to (4), the concentration of filaments far from the bead c_0 scales like $c_0 \sim \xi_0^{-2}$, Eqs. (25) and (26) yield $A_{2,3} \sim c^{-\gamma_{2,3}}$. Our approach predicts $\gamma_{2,3}^{(\mathrm{th})} = 4/3$ in agreement with the experimentally measured values, $\gamma_2^{(\mathrm{exp})} \approx 1.1 \pm 0.3$ and $\gamma_3^{(\mathrm{exp})} \approx 1.4 \pm 0.3$ [14], as well as with the value $\gamma_3^{(\mathrm{sim})} \approx 1.4$ found in the simulations [1].

In order to make estimates of A_i, we used $k_B T \approx 4 \times 10^{-21}$ J, the water viscosity $\eta \approx 10^{-3}$ Pa s, the actin contour length $L \approx 20$ μm, the radius of the bead $R \approx 2.25$ μm equal to that used in the measurements [14,15,42] and the persistent length of actin $L_{\mathrm{p}} \approx 17$ μm [43,44]. Substitution of these values into (24) yields $A_1^{(\mathrm{th})} \approx 23.0$ Pa^{-1} s$^{-3/4}$ at $N = 2$, which agrees with the experimental value $A_1^{(\mathrm{exp})} \approx 27.2 \pm 6.1$ Pa^{-1} s$^{-3/4}$ reported in [14,42].

The network with the actin concentration $c = 11$ μM has a mesh size $\xi_0 \approx 0.5$ μm. The diffusion coefficient can be estimated as $D \sim 10^{-13}$ m^2/s [45]. This estimate of the longitudinal diffusion coefficient of actin agrees with the one which can be obtained from the theoretical prediction [28]. Substituting these parameters into (25) and using the factor χ_2 discussed above one finds $A_2^{(\mathrm{th})} \approx 14.5$ Pa^{-1} s$^{-1/2}$ in good agreement with the value $A_2^{(\mathrm{exp})} \approx 13.2$ Pa^{-1} s$^{-1/2}$ reported in Ref. [15]. Finally, Eq. (26) yields the theoretical prediction for the coefficient in the long-time regime $A_3^{(\mathrm{th})} \approx 1.5$ Pa^{-1} s^{-1}.

It is generally expected that in the long-time regime the bead motion is viscous-like yielding $x(t) = ft/6\pi R \eta_{\mathrm{net}}$ and, thus,

$$A_3 = \eta_{\mathrm{net}}^{-1}, \tag{27}$$

where η_{net} is the (effective) viscosity of the network. The bead displacement (15) indeed depends linearly upon time. However, in the derivation of (19) only the osmotic mechanism was accounted for, while the viscosity was neglected.

The long-time viscosity η_{net} has been measured by force-pulsed magnetic bead microrheometry in Refs. [12] and [46]. In the measurements reported in Ref. [12], however, pulses with maximum durations of 2.5 s were used. The bead motion in the end of such a pulse in this case corresponds to the intermediate, rather than the long-time regime. In Ref. [46], the long-time viscosity $\eta_{\mathrm{net}}^{(\mathrm{exp})} \approx 0.63$ Pa s was reported with 11 s pulses for a network with mesh size of $\xi_0 \approx 0.48$ μm and the bead radius $R = 2.25$ μm. Substituting these data into Eqs. (26) and (27) one finds $A_3^{(\mathrm{th})} \approx 1.3$ Pa^{-1} s^{-1} yielding $\eta_{\mathrm{net}}^{(\mathrm{th})} \approx 0.74$ Pa s in a good agreement with the measured value.

E. Crossover times

We have calculated compliance curves as functions of time for each of the three regimes, and we must consider how they are joined. Compliance is described by a piecewise continous function (23). Transitions from the short-time to the intermediate-time regime, as well as from the intermediate-time to the long-time regime, take place by transition processes which are not accounted for in our approach. Therefore, strictly speaking, we cannot require the compliance to be a continuous function, a smooth function, or a continuous and smooth function. However, the duration of the transition processes is much smaller than that of the corresponding regimes [14], and it is for this reason that we can require that the compliance is a continuous, smooth function of time. The result of this physically based assumption is that it will determine the crossover times at which the compliance curves intersect.

Equating the bead compliance in the short-time and the intermediate-time regimes $A_1\tau_1^{3/4}=A_2\tau_1^{1/2}$ and using (24) and (25), one finds the crossover time τ_1,

$$\tau_1 = \frac{qL_p^{7/3}\xi_0^{32/3}D^2}{N^4R^8}\left(\frac{\eta}{k_BT}\right)^3, \tag{28}$$

where the numerical factor is $q\approx 2.5\times 10^7$. Using the above estimates with $\xi_0\approx 0.5$ μm and $N=2$, one then finds $\tau_1 \approx 0.17$ s in agreement with the observations [14,15].

In the case of the crossover from the intermediate-time to the long-time regime from the assumption of continuity, one finds the relation $A_2\tau_2^{1/2}=A_3\tau_2+B_3$. The assumption of smoothness implies that the bead velocity is continuous, yielding $A_2=2A_3\tau_2^{1/2}$. Solving these equations with respect to the second crossover time τ_2 and the off-set B_3, one finds

$$\tau_2 = \left(\frac{\chi_2}{\chi_3}\right)^2\frac{R^2}{4D}, \quad B_3 = \frac{3\pi\chi_2^2}{2\chi_3}\frac{L_p^{1/3}\xi_0^{8/3}}{k_BT}. \tag{29}$$

Using the above values of the parameters, we find that $B_3 \approx 35.0$ Pa^{-1} and that $\tau_2\approx 23$ s is similar to the observed times which range from 8 to 30 s [14].

F. Elasticity and plasticity of the network response

The motion of the bead gives rise to an increase of the filament concentration in the vicinity in front of it. This results in a compression of the reptation tubes in this region. Small deformations of reptation tubes is the origin of network elasticity at the time scale of the intermediate regime [26,30,47,48]. In our model, the osmotic force (8) originates from both the compression of the tubes and the anisotropy of the distribution of the polymers around the bead. In the beginning of the intermediate-time regime, the bead displacement is comparable to the network mesh size and the network response is elastic. Taking typical values of $A_2 \approx 10$ Pa^{-1} s$^{-1/2}$, $f=10$ pN and $\tau_2\approx 10$ s, one finds a typical bead displacement at the end of the intermediate regime to be $x\approx 7$ μm in agreement with the experimental observations reported in [14,15]. At such values of the bead displacement, the filaments crossing the bead's path are pulled out of their tubes by the bead motion. This implies the irreversibility of the network deformation which thus possesses a plastic component depending upon the extent to which the filaments are pulled from their tubes. In the long-time regime ($t>\tau_2$), the network response becomes viscous.

G. A $x(t)\sim t^{1/2}$ regime in other systems

A binary correlation function and a mean square displacement obeying the power law $\langle x^2(t)\rangle\sim t^{1/2}$ has been observed in actin networks using passive two-bead microrheometry [11]. The network concentration and the time domain in which such a behavior was observed [11] correspond to those in experiments using active probing of actin network [14,15]. We note that this behavior is related to the compliance depending on time like $J(t)\sim t^{1/2}$, as described in our paper in the intermediate-time regime and observed in [14,15]. However, a detailed theory of this phenomenon for the case of passive two-bead microrheometry is beyond the scope of the present paper.

The viscoelastic properties of complex media are often modeled in terms of equivalent mechanical circuits [49]. This approach was applied to analyze the micromechanical behavior of actin networks, the cytoplasm, and cellular membranes [12,46,50–54]. It would be possible to fit the compliance such as that of the actin network reported in [14,15] by an equivalent mechanical circuit. However, an accurate fitting of such a regime would require us to introduce many parameters, via springs and dash pots, which would, however, incorrectly describe the essential physics of the phenomenon. The reason that the compliance increases like $J(t)\sim t^{1/2}$ in the intermediate-time regime is because of the osmotic mechanism arising from polymer compression by the moving bead, and this is fundamentally different from, and cannot be reduced to, the viscoelastic characteristics of the network.

In recent papers [32,33], a phenomenological theory of microrheological measurements was formulated. It is based on a two-fluid hydrodynamic approach [55] in which the actin network was considered as an elastic medium of constant concentration viscously coupled to the penetrating water. As we already discussed at $0<t<\tau_1$, the time is not enough for osmotic pressure to contribute significantly to the bead motion and the approximation of a constant concentration used in [32,33] is applicable. At $t>\tau_1$, the osmotic pressure becomes significant. In this case, our approach may be combined with that of papers [32,33] by accounting for the time-dependent and coordinate-dependent concentration of filaments obeying the diffusion equation.

In general, the $x(t)\sim t^{1/2}$ power law (or, equivalently, the power law $G(\omega)\sim\omega^{1/2}$, describing the dependence of the complex shear modulus of the network on frequency) indicates that the resistance mechanism is dominated by diffusion, but does not indicate the mechanism itself. The power law $G(\omega)\sim\omega^{1/2}$ has been predicted theoretically for flexible polymers, for which $L/L_p\gg 1$ by accounting for the diffusion of their excess lengths along the reptation tubes [28]. In the networks studied both here and in our simulations [1], as well as in those used in measurements [14,15], the polymers are semiflexible, $L/L_p\approx 1.2$, and therefore, the mechanism responsible for the intermediate-time behavior reported in [14,15] differs from that proposed by Morse [28].

Our description of the intermediate-time and long-time regimes is based on taking account of the osmotic pressure on the bead due to the asymmetric distribution of the filaments around it. This phenomenon has already been discussed in several publications in application to systems differing from semiflexible networks.

In the paper [41], the forced motion of a spherical probe particle in a suspension of colloidal particles was studied in the regime of a steady motion. There it was shown that a resistive force arose due to a deformation of the distribution of the colloidal particles around the probe particle.

Kollmann and Nägele developed a theory describing the diffusion of a spherical macroion in a multicomponent colloidal dispersion. They predicted a perturbation $\delta\zeta$ of its short-time friction coefficient ζ by the electrolyte [56]. If the hydrodynamic interactions were "switched off," the

asymptotic behavior of this perturbation would exhibit the dependence $\delta\zeta \sim t^{-1/2}$ on time. However, accounting for the far-field hydrodynamic interactions between the tracer and the microions removes the singularity yielding $\delta\zeta$ to be regular at $t=0$ [56].

Although the entangled network of semiflexible filaments differs considerably from the multicomponent dispersion of spherical colloidal particles studied in Ref. [56], the intermediate-time regime recently observed in actin networks [11,14,15] and predicted by the simulations [1] is qualitatively comparable with the short-time behavior predicted for a colloidal dispersion [56]. In the latter, the hydrodynamic interactions equalize concentrations of colloidal particles in front of and behind the bead and the difference in the osmotic pressure in front of and behind the bead vanishes. In the densely entangled solution of polymers, their low mobility prevents such an equalization of the density. For this reason, the osmotic force exists in the network and (as has been shown here) dominates the resistance of the gel to the bead motion giving rise to the bead motion obeying the law $x(t) \sim t^{1/2}$.

In general, the arising of the osmotic force discussed in this paper requires two conditions: (i) density inhomogeneity of the complex fluid must be formed (giving rise to the spatial inhomogeneity of the osmotic pressure), and (ii) a slow diffusive mode must be responsible for the decay of this inhomogeneity. Such conditions are often fulfilled on the mesoscale in complex fluids. In the recent paper [57], Brochard-Wyart and de Gennes predicted a resistance of adhered biomembranes to an unbinding by account for a transient inhomogeneous osmotic pressure of mobile ligand-receptor pairs.

VI. SUMMARY

Based on our computer simulations [1], we have proposed a mechanism responsible for the resistance of an actin network to the forced motion of an embedded bead. We have shown that the resistance originates in the osmotic pressure exerted on the bead surface by the actin filaments. The pressure arises because the moving bead piles up filaments in front of it, while much fewer filaments are found behind the bead. This mechanism describes the bead motion in both the intermediate-time regime, where the motion obeys the power law $x(t) \sim t^{1/2}$, and the subsequent viscous-like long-time regime in which the bead position varies like $x(t) \sim t$, as well as the dependence of the bead response on the actin concentration recently reported in [14,15].

ACKNOWLEDGMENTS

A.B. was supported by Deutsche Forschungsgemeinschaft Grant No. DFG SA 246/28-4. This work was supported by National Science and Engineering Research Counsul of Canada under a discovery grant to D.A.P.A.B. is grateful to G. Nägele for a useful discussion.

APPENDIX: APPROXIMATE DESCRIPTION OF THE SHORT-TIME REGIME

The enforced bead motion obeying the power law $x(t) \sim t^{3/4}$ has been described theoretically by a mechanism which accounts for a dynamical bending of a filament [21]. The solution was obtained in Ref. [21] in terms of a Green's function. Based on the idea of that paper [21], we give here an approximate calculation of the bead displacement, which enables us to estimate the compliance in the short-time regime and to compare this prediction with our observations in Sec. V.

During the short-time regime of motion, the bead traverses a distance less than the mesh size (~ 0.1 μm [14]) and, therefore, deforms only few filaments. If a local force f is applied to the filament somewhere far from its ends at the initial time then, after a time t, a portion of the filament will be deformed. The length of the deformed part of the filament Λ can be estimated using the equation of filament motion,

$$4\pi\eta \frac{\partial z}{\partial t} = k_B T L_p \frac{\partial^4 z}{\partial s^4} + f\delta(s), \tag{30}$$

where $4\pi\eta$ is an estimate of the friction coefficient, η is the water viscosity, $k_B T L_p$ is the filament bending rigidity, $z = z(s)$ is the filament displacement, s is the coordinate along the filament, and $\delta(s)$ is the δ function. This yields the time dependence of the length of the deformed portion of a filament,

$$\Lambda = \left(\frac{k_B T L_p t}{4\pi\eta} \right)^{1/4}. \tag{31}$$

Assuming that the increase of the length Λ is slower than the filament bending, one can describe the bending by the static equation

$$\partial^4 z/\partial s^4 = 0. \tag{32}$$

with the boundary conditions: (i) $k_B T L_p \partial^3 z/\partial s^3 = f$ describing the force applied at the point $s=0$, (ii) $\partial^2 z/\partial s^2 = 0$ describing the requirement of zero torque applied to the filament by the bead, and (iii) $z(\pm\Lambda) = \partial z(\pm\Lambda)/\partial s = 0$ which approximately describes the filament configuration at $s = \pm\Lambda$. Utilizing the well-known solution for elastic rods [58], one finds the bead displacement x equal to that of the filament at $s=0$: $x = z(0) = f\Lambda^3/192 k_B T L_p$. Making use of (31), one obtains the bead displacement in the form

$$x(t) \sim \frac{t^{3/4}}{192[k_B T L_p (4\pi\eta)^3]^{1/4}} f. \tag{33}$$

If the bead meets N filaments on its way, the result (33) must be multiplied by N. The bead displacement (33) represents an approximation form of the Green's function obtained in [21] taken at $s=0$.

[1] N. Ter-Oganessian *et al.*, Phys. Rev. E **72**, 041510 (2005).
[2] B. Alberts *et al.*, *Molecular Biology of the Cell* (Garland Publishing Inc., New York, 1994).
[3] R. Merkel *et al.*, Biophys. J. **79**, 707 (2000).
[4] L. Vonna *et al.*, J. Cell. Sci. **116**, 785 (2003).
[5] B. Hinner, M. Tempel, E. Sackmann, K. Kroy, and E. Frey, Phys. Rev. Lett. **81**, 2614 (1998).
[6] K. Kroy and E. Frey, Phys. Rev. Lett. **77**, 306 (1996).
[7] J. Käs *et al.*, Biophys. J. **70**, 609 (1996).
[8] P. A. Janmey *et al.*, Biochemistry **27**, 8218 (1988).
[9] F. C. MacKintosh and C. F. Schmidt, Curr. Opin. Colloid Interface Sci. **4**, 300 (1999).
[10] Y. Tseng *et al.*, Curr. Opin. Colloid Interface Sci. **7**, 210 (2002).
[11] J. C. Crocker, M. T. Valentine, E. R. Weeks, T. Gisler, P. O. Kaplan, A. G. Yodh, and D. A. Weitz, Phys. Rev. Lett. **85**, 888 (2000).
[12] F. Ziemann, J. Rädler, and E. Sackmann, Biophys. J. **66**, 2210 (1994).
[13] F. G. Schmidt, B. Hinner, and E. Sackmann, Phys. Rev. E **61**, 5646 (2000).
[14] J. Uhde, Ph.D. thesis, Technical University Munich, 2004 (unpublished), http://tumb1.biblio.tu-muenchen.de/publ/diss/ph/2004/uhde.html
[15] J. Uhde, W. Feneberg, N. Ter-Oganessian, E. Sackmann, and A. Boulbitch, Phys. Rev. Lett. **94**, 198102 (2005).
[16] T. Odijk, Macromolecules **16**, 1340 (1983).
[17] M. Dijkstra, D. Frenkel, and H. N. W. Lekkerkerker, Physica A **193**, 374 (1993).
[18] F. C. MacKintosh, J. Käs, and P. A. Janmey, Phys. Rev. Lett. **75**, 4425 (1995).
[19] T. W. Burkhardt, J. Phys. A **28**, L629 (1995).
[20] T. W. Burkhardt, J. Phys. A **30**, L167 (1997).
[21] F. Amblard, A. C. Maggs, B. Yurke, A. N. Pargellis, and S. Leibler, Phys. Rev. Lett. **77**, 4470 (1996).
[22] K. Kroy and E. Frey, Phys. Rev. E **55**, 3092 (1997).
[23] R. Granek, J. Phys. II **7**, 1761 (1997).
[24] F. Gittes, B. Schnurr, P. D. Olmsted, F. C. Mockintosh, and C. F. Schmidt, Phys. Rev. Lett. **79**, 3286 (1997).
[25] F. Gittes and F. C. MacKintosh, Phys. Rev. E **58**, R1241 (1998).
[26] D. C. Morse, Macromolecules **31**, 7030 (1998).
[27] D. C. Morse, Phys. Rev. E **58**, R1237 (1998).
[28] D. C. Morse, Macromolecules **31**, 7044 (1998).
[29] D. C. Morse, Macromolecules **32**, 5934 (1999).
[30] A. C. Maggs, Phys. Rev. E **57**, 2091 (1998).
[31] D. J. Bicout and T. W. Burkhardt, J. Phys. A **34**, 5745 (2001).
[32] A. J. Levine and T. C. Lubensky, Phys. Rev. Lett. **85**, 1774 (2000).
[33] A. J. Levine and T. C. Lubensky, Phys. Rev. E **63**, 041510 (2001).
[34] A. J. Levine and T. C. Lubensky, Phys. Rev. E **65**, 011501 (2002).
[35] W. Helfrich and W. Harbich, Chem. Scr. **25**, 32 (1985).
[36] L. D. Landau and E. M. Lifshitz, *Statistical Physics* (Pergamon Press, Oxford, 1985).
[37] M. A. Dichtl and E. Sackmann, New J. Phys. **1**, 18.1/18.11 (1999).
[38] J. L. McGrath, J. H. Hartwig, and S. C. Kuo, Biophys. J. **79**, 3258 (2000).
[39] D. T. Chen, E. R. Weeks, J. C. Crocker, M. F. Islam, R. Verma, J. Gruber, A. J. Levine, T. C. Lubensky, and A. G. Yodh, Phys. Rev. Lett. **90**, 108301 (2003).
[40] B. S. Chae and E. M. Furst, Langmuir **21**, 3084 (2005).
[41] H. N. W. Lekkerkerker and J. K. G. Dhont, J. Chem. Phys. **80**, 5790 (1984).
[42] J. Uhde, N. Ter-Oganessian, D. A. Pink *et al.* (unpublished).
[43] A. Ott, M. Magnasco, A. Simon, and A. Libchaber, Phys. Rev. E **48**, R1642 (1993).
[44] F. Gittes *et al.*, J. Cell. Biochem. **120**, 923 (1993).
[45] M. Dichtl and E. Sackmann (unpublished).
[46] F. Schmidt, Ph.D. thesis, Technical University, Munich, 1999 (unpublished).
[47] H. Isambert and A. C. Maggs, Macromolecules **29**, 1036 (1996).
[48] E. Frey, Adv. Solid State Phys. **41**, 345 (2001).
[49] N. W. Tschoegl, *The Phenomenological Theory of Linear Viscoelastic Behavior* (Springer-Verlag, Berlin, 1989).
[50] A. R. Bausch *et al.*, Biophys. J. **75**, 2038 (1998).
[51] A. R. Bausch, W. Möller, and E. Sackmann, Biophys. J. **76**, 573 (1999).
[52] M. A. Dichtl and E. Sackmann, Proc. Natl. Acad. Sci. U.S.A. **99**, 6533 (2002).
[53] W. Feneberg, M. Westphal, and E. Sackmann, Eur. Biophys. J. **30**, 284 (2001).
[54] F. G. Schmidt, F. Ziemann, and E. Sackmann, Eur. Biophys. J. **24**, 348 (1996).
[55] H. C. Brinkman, Appl. Sci. Res., Sect. A **A1**, 27 (1947).
[56] M. Kollmann and G. Nagele, J. Chem. Phys. **113**, 7672 (2000).
[57] F. Brochard-Wyart and P. G. De Gennes, Proc. Natl. Acad. Sci. U.S.A. **99**, 7854 (2002).
[58] L. D. Landau and E. M. Lifshitz, *Theory of Elasticity* (Pergamon Press, Oxford, 1986).